Unitary ESPRIT: How to Obtain Increased Estimation Accuracy with a Reduced Computational Burden

Martin Haardt, *Student Member, IEEE* and Josef A. Nossek, *Fellow, IEEE*

***Abstract*—ESPRIT is a high-resolution signal parameter estimation technique based on the translational invariance structure of a sensor array. Previous ESPRIT algorithms do not use the fact that the operator representing the phase delays between the two subarrays is unitary. Here, we present a simple and efficient method to constrain the estimated phase factors to the unit circle, if centro-symmetric array configurations are used. Unitary ESPRIT, the resulting closed-form algorithm, has an ESPRIT-like structure except for the fact that it is formulated in terms of real-valued computations throughout. Since the dimension of the matrices is not increased, this completely real-valued algorithm achieves a substantial reduction of the computational complexity. Furthermore, Unitary ESPRIT incorporates forward-backward averaging, leading to an improved performance compared to the standard ESPRIT algorithm, especially for correlated source signals. Like standard ESPRIT, Unitary ESPRIT offers an inexpensive possibility to reconstruct the impinging wavefronts (signal copy). These signal estimates are more accurate, since Unitary ESPRIT improves the underlying signal subspace estimates. Simulations confirm that, even for uncorrelated signals, the standard ESPRIT algorithm needs twice the number of snapshots to achieve a precision comparable to that of Unitary ESPRIT. Thus, Unitary ESPRIT provides increased estimation accuracy with a reduced computational burden.**

I. Introduction

THE recovery of signal parameters from noisy observations is a fundamental problem in (real-time) array signal processing. Due to their simplicity and high-resolution capability, ESPRIT-like subspace estimation schemes have been attracting considerable attention. Their parameter estimates are obtained by exploiting the *rotational* invariance structure of the signal subspace, induced by the *translational* invariance structure of the associated sensor array. This can be achieved without computation or search of any spectral measure [15], [17]. Unitary ESPRIT achieves even more accurate results than previous ESPRIT techniques by taking advantage of the unit magnitude property of the phase factors that represent the phase delays between the two subarrays [4]. It has been shown in [12] that constraining the phase factors to the unit circle can also give some improvement for correlated sources. For centro-symmetric sensor arrays with a translational invariance structure, Unitary ESPRIT provides a very simple and efficient solution to this task.

Although Unitary ESPRIT effectively doubles the number of of data samples, the computational complexity is reduced by transforming the required rank-revealing factorizations of complex matrices into decompositions of *real-valued* matrices of the *same size*. Thus, we obtain increased estimation accuracy with a reduced computational load. This reduction can be achieved by constructing invertible transformations that map centro-Hermitian matrices to real matrices. These transformations have been introduced in Lee's pioneering work on centro-Hermitian matrices [10]. More than a decade later, her results were used to transform the complex covariance matrix of a uniform linear array (ULA) into a real matrix of the same size [8] to reduce the computational load of adaptive beamforming schemes [9]. In this paper, we use more general centro-symmetric array configurations that have been receiving increased attention lately [22]. We derive an efficient square root version of Unitary ESPRIT that only requires real-valued computations from start to finish, by operating directly on the data instead of "squaring" it to obtain sample covariance matrices. It is well known that benefits result from smaller matrix conditioning numbers [15]. With infinite precision, both strategies would be the same, whether eigendecompositions or singular value decompositions (SVD's) are used. Finite precision arithmetic, however, is employed in practical applications. Therefore, numerical issues like round-off error and overflow are potential problems to be aware of when covariance matrices are estimated. In addition to this square root approach, we also describe an alternative real-valued covariance approach, cf. Remark 1, which turns out to be more efficient than the one proposed in [8] and [24].

In the presence of additive noise, the computation of an optimal signal subspace estimate requires an SVD or an eigenvalue decomposition (EVD), which is computationally expensive, since $\mathcal{O}(M^3)$ operations are necessary to update the SVD or EVD if a new sample vector of dimension M arrives. Therefore, a number of alternative decompositions have been proposed to estimate the signal subspace in a computationally more efficient way. Examples include the rank-revealing QR decomposition [1], [2], the rank-revealing URV decomposition [11], [18], or a new Schur-type method for subspace estimation [3], [9]. These approximation techniques are computationally more efficient and well suited for a parallel (systolic) implementation, but they involve a certain

Manuscript received June 8, 1994; revised August 30, 1994. The associate editor coordinating the review of this paper and approving it for publication was Prof. Keshab Parhi.

The authors are with the Institute of Network Theory and Circuit Design, Technical University of Munich, Munich, Germany.

IEEE Log Number 9410301.

loss of accuracy that can be compensated by combining them with Unitary ESPRIT, yielding not only improved estimation accuracy, but also completely real-valued algorithms. In [5], it is shown how Unitary Schur ESPRIT dramatically improves the performance of the new Schur-type method, an adaptive subspace estimation scheme with a computational structure and complexity similar to that of a QR decomposition, except for the fact that plane and hyperbolic rotations are used. In this case, the required rank decision, i.e., an estimate of the number of signals, is automatic, and updating as well as downdating are straightforward. The fully real-valued Unitary ESPRIT concept can also be extended to spatially smoothed forward-backward estimation schemes [6], [13], [14] and is applicable to many other subspace estimation techniques (see [20] for an excellent overview). The results are comparable to the advantages obtained by operating in beamspace [24] without the necessity of converting the data from element space to beamspace.

This paper is organized as follows. It starts with a review of the definition and basic properties of centro-Hermitian matrices. These properties will be used to derive the real-valued implementation of Unitary ESPRIT. A brief review of the standard ESPRIT algorithm is given in chapter III. It can be seen as a generalization of the matrix pencil method [7]. Chapter IV introduces the Unitary ESPRIT concept for centro-symmetric array structures. In Section IV-B we show how all three required rank-revealing factorizations can be transformed into decompositions of *real-valued* matrices of the *same size* yielding a completely real algorithm. A new reliability test, which is a substantial improvement of current high-resolution array signal processing and spectral estimation techniques, is presented in Section IV-C. Further simplifications of the algorithm are derived in Section IV-D, before a summary of Unitary ESPRIT concludes the chapter (Section IV-E). Finally, computer simulations compare the performance of Unitary ESPRIT with that of the well-known standard ESPRIT algorithm (Section V).

II. Centro-Hermitian Matrices

First of all, let us introduce our notation and review the definition and the basic properties of centro-Hermitian matrices that have been derived by Lee [10]. Throughout this paper, column vectors and matrices are denoted by lower case and upper case boldfaced letters, respectively. $\boldsymbol{\Pi}_p$ is the $p \times p$ exchange matrix with ones on its antidiagonal and zeros elsewhere

$$\boldsymbol{\Pi}_p = \begin{bmatrix} & & 1 \\ & \iddots & \\ 1 & & \end{bmatrix} \in \mathbb{R}^{p \times p}.$$

Since $\boldsymbol{\Pi}_p$ is a symmetric permutation matrix, it is involutorial, i.e., $\boldsymbol{\Pi}_p^2 = \boldsymbol{I}_p$. With this notation, we can define centro-Hermitian matrices in analogy to centro-symmetric matrices.

Definition 1: A complex matrix $\boldsymbol{M} \in \mathbb{C}^{p \times q}$ is called *centro-Hermitian* if

$$\boldsymbol{\Pi}_p \overline{\boldsymbol{M}} \boldsymbol{\Pi}_q = \boldsymbol{M} \tag{1}$$

where the overbar denotes complex conjugation without transposition.

Centro-Hermitian matrices of size $p \times q$ form a $p \cdot q$-dimensional linear space over $\mathbb{R}$ [10]. To show how centro-Hermitian matrices can be mapped to matrices with real entries, Lee defines left $\boldsymbol{\Pi}$-real matrices in the following fashion.

Definition 2 [10]: Matrices $\boldsymbol{Q} \in \mathbb{C}^{p \times q}$ satisfying

$$\boldsymbol{\Pi}_p \overline{\boldsymbol{Q}} = \boldsymbol{Q} \tag{2}$$

are *left $\boldsymbol{\Pi}$-real.*

The unitary matrices

$$\boldsymbol{Q}_{2n} = \frac{1}{\sqrt{2}} \begin{bmatrix} \boldsymbol{I}_n & j\boldsymbol{I}_n \\ \boldsymbol{\Pi}_n & -j\boldsymbol{\Pi}_n \end{bmatrix} \tag{3}$$

$$\boldsymbol{Q}_{2n+1} = \frac{1}{\sqrt{2}} \begin{bmatrix} \boldsymbol{I}_n & \boldsymbol{0} & j\boldsymbol{I}_n \\ \boldsymbol{0}^T & \sqrt{2} & \boldsymbol{0}^T \\ \boldsymbol{\Pi}_n & \boldsymbol{0} & -j\boldsymbol{\Pi}_n \end{bmatrix} \tag{4}$$

for example, are left $\boldsymbol{\Pi}$-real of even and odd order, respectively. More left $\boldsymbol{\Pi}$-real matrices can be obtained by post-multiplying a left $\boldsymbol{\Pi}$-real matrix $\boldsymbol{Q}$ by an arbitrary real matrix $\boldsymbol{R}$, i.e., every matrix $\boldsymbol{QR}$ is left $\boldsymbol{\Pi}$-real. Now, we are in a position to state Lee's main result, which establishes an automorphism between centro-Hermitian and real matrices.

Theorem 1 [10]: Let $\boldsymbol{T}_p$ and $\boldsymbol{U}_q$ denote arbitrary nonsingular left $\boldsymbol{\Pi}$-real matrices of size $p \times p$ and $q \times q$, respectively. Then, the bijective mapping

$$\varphi: \boldsymbol{M} \mapsto \boldsymbol{T}_p^{-1} \boldsymbol{M} \boldsymbol{U}_q$$

maps the set of all $p \times q$ centro-Hermitian matrices onto $\mathbb{R}^{p \times q}$, the set of all real matrices of the same size.

This theorem can, for instance, be used to calculate the singular value decomposition (SVD) of a centro-Hermitian matrix $\boldsymbol{M} \in \mathbb{C}^{p \times q}$.

Corollary 1: Let $\boldsymbol{M}$ be centro-Hermitian, and assume that the SVD of $\varphi_Q(\boldsymbol{M}) = \boldsymbol{Q}_p^H \boldsymbol{M} \boldsymbol{Q}_q \in \mathbb{R}^{p \times q}$ is given by $\varphi_Q(\boldsymbol{M}) = \boldsymbol{U}_\varphi \boldsymbol{\Sigma}_\varphi \boldsymbol{V}_\varphi^H$, where the matrices $\boldsymbol{Q}_p$ and $\boldsymbol{Q}_q$ are unitary as well as left $\boldsymbol{\Pi}$-real. Then, an SVD[1] of $\boldsymbol{M}$ is obtained as

$$\boldsymbol{M} = (\boldsymbol{Q}_p \boldsymbol{U}_\varphi) \boldsymbol{\Sigma}_\varphi (\boldsymbol{V}_\varphi^H \boldsymbol{Q}_q^H) \tag{5}$$

where the left and right singular vectors of $\boldsymbol{M}$ are left $\boldsymbol{\Pi}$-real.

Proof: The first part follows from the unitary nature of $\boldsymbol{Q}_p$ and $\boldsymbol{Q}_q$, the second from the fact that the singular vectors of a real matrix are real. ■

For future reference, we consider an efficient computation of a particular transformation $\mathcal{T}(\cdot)$. It transforms an arbitrary complex matrix $\boldsymbol{G} \in \mathbb{C}^{p \times q}$ into a real $p \times 2q$ matrix, denoted by $\mathcal{T}(\boldsymbol{G})$. Notice that for every matrix $\boldsymbol{G}$, the matrix

$$[\boldsymbol{G} \quad \boldsymbol{\Pi}_p \overline{\boldsymbol{G}} \boldsymbol{\Pi}_q] \in \mathbb{C}^{p \times 2q}$$

is centro-Hermitian. Thus, the matrix

$$\begin{aligned} \mathcal{T}(\boldsymbol{G}) &\stackrel{\text{def}}{=} \varphi_Q([\boldsymbol{G} \quad \boldsymbol{\Pi}_p \overline{\boldsymbol{G}} \boldsymbol{\Pi}_q]) \\ &= \boldsymbol{Q}_p^H [\boldsymbol{G} \quad \boldsymbol{\Pi}_p \overline{\boldsymbol{G}} \boldsymbol{\Pi}_q] \boldsymbol{Q}_{2q} \end{aligned} \tag{6}$$

[1] Recall that the SVD of a complex matrix is unique up to a unitary diagonal scaling matrix, if all singular values are distinct.

is always real according to Theorem 1. Consider the case where the left Π-real matrices Q_p and Q_{2q} are chosen according to (3) or (4). Furthermore, let G be partitioned as

$$G = \begin{bmatrix} G_1 \\ g^T \\ G_2 \end{bmatrix}$$

where the block matrices G_1 and G_2 should have the same size. Obviously, the row vector g^T must be dropped if p is even. Then, straightforward calculations show that the desired real-valued matrix (6) can be expressed as

$$\mathcal{T}(G) = \begin{bmatrix} \mathrm{Re}\{G_1 + \Pi\overline{G}_2\} & -\mathrm{Im}\{G_1 - \Pi\overline{G}_2\} \\ \sqrt{2}\cdot\mathrm{Re}\{g^T\} & -\sqrt{2}\cdot\mathrm{Im}\{g^T\} \\ \mathrm{Im}\{G_1 + \Pi\overline{G}_2\} & \mathrm{Re}\{G_1 - \Pi\overline{G}_2\} \end{bmatrix}. \quad (7)$$

Here, $\mathrm{Re}\{\cdot\}$ and $\mathrm{Im}\{\cdot\}$ denote the real and the imaginary part, respectively. Once again, if p is odd, the center row of (7) should be dropped. Then, an efficient computation of $\mathcal{T}(G) \in \mathbb{R}^{p\times 2q}$ from the complex matrix G only requires $p \times 2q$ real additions.

III. Standard ESPRIT

A. Standard ESPRIT Scenario

Consider the standard ESPRIT scenario [15], [17], i.e., an M-element sensor array composed of m pairs of pairwise identical, but displaced sensors (doublets). Let Δ denote the distance between the two subarrays. Incident on both subarrays are d narrow-band noncoherent planar wavefronts

$$s_k(t_n) = u(t_n)e^{j(\omega_0 t_n + v(t_n))}, \qquad 1 \le k \le d \le m$$

with signal propagation velocity c and a common center frequency ω_0. The d impinging signals are combined to a signal vector $s(t_n)$. Assume, for the moment, that the two subarrays do not share any elements, i.e., they do not overlap. Then, the total number of sensors equals $M = 2m$ and the uncorrupted signals received at the two subarrays have the following form:

$$x(t_n) = \begin{bmatrix} x_1(t_n) \\ x_2(t_n) \end{bmatrix} = \begin{bmatrix} A \\ A\Phi \end{bmatrix} s(t_n) = A_G s(t_n). \quad (8)$$

$A_G \in \mathbb{C}^{M\times d}$ and $A \in \mathbb{C}^{m\times d}$ are the steering matrices of the whole array configuration (global array steering matrix) and the first subarray, respectively. Notice that the kth columns of both array steering matrices depend on the direction of arrival (DOA) θ_k of the kth source relative to the displacement between the two subarrays.[2] Furthermore

$$\Phi = \mathrm{diag}\{\phi_k\}_{k=1}^{d} \in \mathbb{C}^{d\times d}$$

is a diagonal matrix of the phase delays between the sensor doublets for the d wavefronts. Its diagonal elements, the phase factors ϕ_k, are given by

$$\phi_k = e^{-j\omega_0 \Delta \sin\theta_k / c} \stackrel{\mathrm{def}}{=} e^{j\mu_k}, \qquad 1 \le k \le d. \quad (9)$$

[2] $\theta_k = 0$ corresponds to the direction perpendicular to Δ.

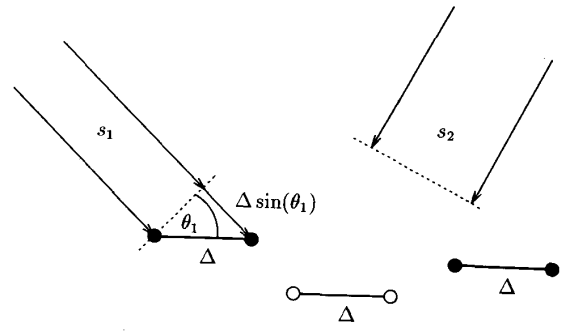

Fig. 1. Planar array composed of $m = 3$ pairwise identical but displaced sensors (doublets).

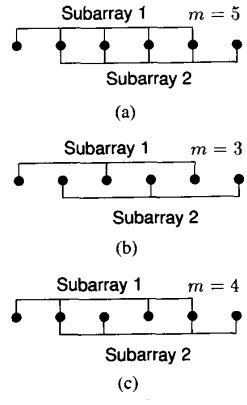

Fig. 2. Three different subarray choices for a uniform linear array (ULA) of $M = 6$ identical sensors. (a) Maximum overlap ($m = 5$); (b) interleaved ($m = 3$); (c) mixed ($m = 4$).

B. More Structured Array Geometries

Recall that every row of A_G corresponds to an element of the sensor array. In the case of overlapping subarrays, a particular subarray configuration is described by selection matrices that choose m elements of $x(t_n) \in \mathbb{C}^M$, where $m < M$ is the number of elements in each subarray. Let J_1 and J_2 be $m \times M$ selection matrices that assign elements of $x(t_n)$ to the subarrays one and two, respectively. Fig. 2, for example, displays three different subarray choices for a uniform linear array (ULA) of $M = 6$ identical sensors.

In general, the two selection matrices are chosen to be centro-symmetric with respect to one another, i.e.

$$J_2 = \Pi_m J_1 \Pi_M \quad (10)$$

a property that plays a key role in the derivation of the fully real implementation of Unitary ESPRIT, *cf.* Section IV-B. Therefore, the combined selection matrix

$$J \stackrel{\mathrm{def}}{=} \begin{bmatrix} J_1 \\ J_2 \end{bmatrix} \in \mathbb{R}^{2m\times M}$$

is centro-Hermitian, i.e. $\Pi_{2m} J \Pi_M = J$.

C. General ESPRIT Principle

By collecting $N \ge d$ snapshots from each sensor, $1 \le n \le N$, measurement matrices X_1, X_2, X and a signal matrix S

are formed, obeying

$$\boldsymbol{JX} = \boldsymbol{J}[\boldsymbol{x}(t_1) \quad \boldsymbol{x}(t_2) \quad \cdots \quad \boldsymbol{x}(t_N)] = \begin{bmatrix} \boldsymbol{X}_1 \\ \boldsymbol{X}_2 \end{bmatrix} = \begin{bmatrix} \boldsymbol{A} \\ \boldsymbol{A\Phi} \end{bmatrix} \boldsymbol{S}. \tag{11}$$

It is easy to see that every row in $\boldsymbol{X}$ corresponds to an element of the sensor array. Equation (11) implies that $\boldsymbol{X}_1, \boldsymbol{X}_2$, and $\boldsymbol{X}$ are rank-deficient, namely rank $\boldsymbol{X}_1$ = rank $\boldsymbol{X}_2$ = rank $\boldsymbol{X} = d$. Thus, the d columns of

$$\begin{bmatrix} \boldsymbol{C}_1 \\ \boldsymbol{C}_2 \end{bmatrix} = \begin{bmatrix} \boldsymbol{X}_1 \\ \boldsymbol{X}_2 \end{bmatrix} \boldsymbol{P}_{\text{col}} = \begin{bmatrix} \boldsymbol{A} \\ \boldsymbol{A\Phi} \end{bmatrix} \boldsymbol{SP}_{\text{col}}$$

form a basis for the column space of $\boldsymbol{X}$ if

$$\boldsymbol{SP}_{\text{col}} \in \text{GL}(d). \tag{12}$$

Here, $\text{GL}(d) \subset \mathbb{C}^{d \times d}$ denotes the general linear group of all nonsingular matrices of dimension $d \times d$. Observe that the column space or range of $\boldsymbol{JX}$, range $\boldsymbol{JX} \subset \mathbb{C}^{2m}$, is usually called *signal subspace*. In the same way, the d rows of

$$[\boldsymbol{\Gamma}_1 \quad \boldsymbol{\Gamma}_2] = \boldsymbol{P}_{\text{row}}[\boldsymbol{C}_1 \quad \boldsymbol{C}_2] = \boldsymbol{P}_{\text{row}}\boldsymbol{A}[\boldsymbol{SP}_{\text{col}} \quad \boldsymbol{\Phi SP}_{\text{col}}]$$

form a basis for the row space of $[\boldsymbol{C}_1 \quad \boldsymbol{C}_2]$ if

$$\boldsymbol{P}_{\text{row}}\boldsymbol{A} \in \text{GL}(d). \tag{13}$$

Therefore, the rank-reducing numbers of the matrix pencil

$$\boldsymbol{\Gamma}_2 - \lambda\boldsymbol{\Gamma}_1 = \boldsymbol{P}_{\text{row}}\boldsymbol{A}(\boldsymbol{\Phi} - \lambda\boldsymbol{I}_d)\boldsymbol{SP}_{\text{col}}$$

are the diagonal elements of $\boldsymbol{\Phi}$ (phase factors) and can be calculated as the generalized eigenvalues of the matrix pair $(\boldsymbol{\Gamma}_2, \boldsymbol{\Gamma}_1)$.

Due to these observations, the ESPRIT algorithm reduces to choosing the appropriate compression matrices that define the required bases. In the absence of noise (the case discussed so far), any matrices $\boldsymbol{P}_{\text{col}}$ and $\boldsymbol{P}_{\text{row}}$ satisfying (12) and (13) will do the job. With noisy measurements, however, we are faced with the problem of estimating the signal subspace and its dimension.

D. SVD-Based Subspace Estimate

The most robust way to estimate the required bases is to compute the singular value decomposition (SVD) of

$$\tilde{\boldsymbol{X}} = [\boldsymbol{U}_s \quad \boldsymbol{U}_{\text{o}}] \begin{bmatrix} \boldsymbol{\Sigma}_s & \\ & \boldsymbol{\Sigma}_{\text{o}} \end{bmatrix} \begin{bmatrix} \boldsymbol{V}_{\text{s}}^H \\ \boldsymbol{V}_{\text{o}}^H \end{bmatrix} \tag{14}$$

where $\tilde{\boldsymbol{X}}$ denotes the measurement matrix $\boldsymbol{X}$ corrupted by additive, spatially uncorrelated[3] noise, $\boldsymbol{\Sigma}_s$ contains its d dominant singular values, and the unitary matrices $\boldsymbol{U}$ and $\boldsymbol{V}$ are partitioned accordingly. Then, the *best* rank d approximation of $\tilde{\boldsymbol{X}}$ in the Frobenius-norm is given by $\hat{\boldsymbol{X}} = \boldsymbol{U}_s\boldsymbol{\Sigma}_s\boldsymbol{V}_s^H$. In other words, our low rank estimate of $\tilde{\boldsymbol{X}}$ is the matrix $\hat{\boldsymbol{X}}$ satisfying

$$\|\tilde{\boldsymbol{X}} - \hat{\boldsymbol{X}}\|_F = \min_{\text{rank } Y \le d} \|\tilde{\boldsymbol{X}} - \boldsymbol{Y}\|_F. \tag{15}$$

[3]If the spatial covariance matrix of the additive noise is known up to a scalar factor, the SVD can be replaced by the generalized or quotient SVD (QSVD), as described in [17].

A basis for the estimated signal subspace is determined from the d dominant left singular vectors according to

$$\boldsymbol{JU}_s = \begin{bmatrix} \boldsymbol{C}_1 \\ \boldsymbol{C}_2 \end{bmatrix}.$$

Then, a unitary basis for the row space of $[\boldsymbol{C}_1 \quad \boldsymbol{C}_2]$ can also be obtained by computing its SVD (*total least squares* approach). However, it is less expensive to use $\boldsymbol{P}_{\text{row}} = \boldsymbol{C}_1^H$, which corresponds to the standard *least squares* solution of the overdetermined set of equations

$$\boldsymbol{C}_1\boldsymbol{\Psi} \approx \boldsymbol{C}_2 \tag{16}$$

followed by an eigendecomposition of $\boldsymbol{\Psi} = \boldsymbol{\Gamma}_1^{-1}\boldsymbol{\Gamma}_2$.

IV. Unitary ESPRIT

A. Multiple Invariance Structure

Unitary ESPRIT is applicable to *centro-symmetric* array configurations. A sensor array is called centro-symmetric [22] if its element locations are symmetric with respect to the centroid and the complex characteristics of paired elements are the same. Their global array steering matrix $\boldsymbol{A}_G$, therefore, satisfies

$$\boldsymbol{\Pi}_M\overline{\boldsymbol{A}}_G = \boldsymbol{A}_G\boldsymbol{\Lambda}_G \tag{17}$$

for some unitary diagonal matrix $\boldsymbol{\Lambda}_G \in \mathbb{C}^{d \times d}$. Notice that the matrix $\boldsymbol{A}_G\boldsymbol{\Lambda}_G^{1/2}$ is left $\boldsymbol{\Pi}$-real.

Uniform linear arrays, for example, the most common arrays used in practice, are centro-symmetric. It is well known that the analogy between array signal processing and time series analysis (harmonic retrieval) can be obtained through uniform linear arrays (ULA's) by interpreting them as uniform sampling of a time series [16].

The centro-symmetry of the global sensor array $\boldsymbol{A}_G$ and (10) imply that the steering matrices of both subarrays are also centro-symmetric, i.e.

$$\boldsymbol{\Pi}_m\overline{\boldsymbol{A}} = \boldsymbol{A\Lambda} \quad \text{with} \quad \boldsymbol{\Lambda} = \boldsymbol{\Phi\Lambda}_G.$$

Without additive noise, the Unitary ESPRIT data matrix

$$\boldsymbol{Z} \stackrel{\text{def}}{=} [\boldsymbol{X} \quad \boldsymbol{\Pi}_M\overline{\boldsymbol{X}}]$$

admits the factorization

$$\boldsymbol{JZ} = \begin{bmatrix} \boldsymbol{X}_1 & \boldsymbol{\Pi}_m\overline{\boldsymbol{X}}_2 \\ \boldsymbol{X}_2 & \boldsymbol{\Pi}_m\overline{\boldsymbol{X}}_1 \end{bmatrix} = \begin{bmatrix} \boldsymbol{A} \\ \boldsymbol{A\Phi} \end{bmatrix} [\boldsymbol{S} \quad \boldsymbol{\Phi}^{-1}\boldsymbol{\Lambda}\overline{\boldsymbol{S}}] \tag{18}$$

which is easily seen by using the centro-symmetry of the subarrays and the unitary nature of $\boldsymbol{\Phi}$. Thus, $\boldsymbol{Z}$ is also rank-deficient, namely rank $\boldsymbol{Z} = d$. Equations (11) and (18) show that Unitary ESPRIT essentially doubles the number of available measurements from N to $2N$. Increased estimation accuracy can, therefore, be achieved by replacing the measurement matrix $\boldsymbol{X} \in \mathbb{C}^{M \times N}$ of the standard ESPRIT formulation (11) by $\boldsymbol{Z} \in \mathbb{C}^{M \times 2N}$, which corresponds to forward-backward averaging of the data.

B. Real Implementation

Due to the special algebraic structure of the noise-corrupted data matrix $\tilde{\boldsymbol{Z}}$ and the structure of the subsequent total least squares (TLS) problem, the computational complexity of Unitary ESPRIT can be reduced significantly. This is achieved by transforming the three (complex-valued) rank-revealing factorizations,

- the subspace estimation step
- the subsequent total least squares problem
- the final eigenvalue decomposition (EVD)

into factorizations of *real-valued* matrices of the *same size*. Thus, real-valued computations can be maintained for all steps of the Unitary ESPRIT algorithm. The following three propositions derive the required transformations by taking advantage of the mapping between centro-Hermitian and real matrices, cf. Section II. In Remark 3, we also show how the real-valued total least squares problem can be replaced by a real-valued least squares (LS) problem.

Proposition 1—Signal Subspace Estimation: The principal subspace of $\tilde{\boldsymbol{Z}} \in \mathbb{C}^{M\times 2N}$ (and, therefore, also the principal subspace of $\boldsymbol{J}\tilde{\boldsymbol{Z}}$) can be obtained through a rank-revealing factorization of the real matrix $\mathcal{T}(\tilde{\boldsymbol{X}}) \in \mathbb{R}^{M\times 2N}$, where the transformation $\mathcal{T}(\cdot)$ is defined in (6). Then, the complex matrices $\boldsymbol{C}_1$ and $\boldsymbol{C}_2$, spanning the estimated signal subspace, obey

$$\boldsymbol{C}_2 = \boldsymbol{\Pi}_m \overline{\boldsymbol{C}}_1. \tag{19}$$

Proof: By post-multiplying the noise-corrupted matrix $\tilde{\boldsymbol{Z}}$ with a unitary permutation matrix we obtain a centro-Hermitian matrix in the following fashion:

$$\tilde{\boldsymbol{Z}}_{\mathrm{CH}} = \tilde{\boldsymbol{Z}}\begin{bmatrix} \boldsymbol{I}_N & \\ & \boldsymbol{\Pi}_N \end{bmatrix} = [\tilde{\boldsymbol{X}} \quad \boldsymbol{\Pi}_M \overline{\tilde{\boldsymbol{X}}} \boldsymbol{\Pi}_N]. \tag{20}$$

According to Corollary 1, a rank-revealing factorization of $\tilde{\boldsymbol{Z}}_{\mathrm{CH}}$ can, thus, be obtained through an SVD of the real matrix

$$\varphi_Q(\tilde{\boldsymbol{Z}}_{\mathrm{CH}}) = \boldsymbol{Q}_M^H \tilde{\boldsymbol{Z}}_{\mathrm{CH}} \boldsymbol{Q}_{2N} = \mathcal{T}(\tilde{\boldsymbol{X}}) \tag{21}$$

which proves the first part of this proposition. Let the d dominant left singular vectors of $\varphi_Q(\tilde{\boldsymbol{Z}}_{\mathrm{CH}})$ be denoted by $\boldsymbol{E}_s \in \mathbb{R}^{M\times d}$. Then, the d dominant left singular vectors of $\tilde{\boldsymbol{Z}}_{\mathrm{CH}}$ as well as $\tilde{\boldsymbol{Z}}$ are given by $\boldsymbol{Q}_M \boldsymbol{E}_s$. Therefore, the matrix

$$\begin{bmatrix} \boldsymbol{C}_1 \\ \boldsymbol{C}_2 \end{bmatrix} = \begin{bmatrix} \boldsymbol{J}_1 \\ \boldsymbol{J}_2 \end{bmatrix} \boldsymbol{Q}_M \boldsymbol{E}_s$$

provides a basis for the estimated signal subspace. With (10) and the left $\boldsymbol{\Pi}$-realness of $\boldsymbol{Q}_M$ we, finally, get the desired result:

$$\begin{aligned} \boldsymbol{\Pi}_m \overline{\boldsymbol{C}}_1 &= \boldsymbol{\Pi}_m \boldsymbol{J}_1 \overline{\boldsymbol{Q}}_M \boldsymbol{E}_s \\ &= \boldsymbol{\Pi}_m \boldsymbol{\Pi}_m \boldsymbol{J}_2 \boldsymbol{\Pi}_M \overline{\boldsymbol{Q}}_M \boldsymbol{E}_s \\ &= \boldsymbol{J}_2 \boldsymbol{Q}_M \boldsymbol{E}_s = \boldsymbol{C}_2. \end{aligned}$$

■

Proposition 2—Total Least Squares Problem: The complex-valued SVD of size $m \times 2d$ that solves the total least squares (TLS) problem $\boldsymbol{C}_1\boldsymbol{\Psi} \approx \boldsymbol{C}_2$, which is associated with Unitary ESPRIT, can be transformed into an SVD of the real matrix $\mathcal{T}(\boldsymbol{C}_1) \in \mathbb{R}^{m\times 2d}$, where the transformation $\mathcal{T}(\cdot)$ is defined in (6). Moreover, the eigenvalues ϕ_k of the resulting TLS solution $\Psi_{\mathrm{TLS}} \in \mathbb{C}^{d\times d}$ will be symmetric with respect to the unit circle, i.e., there are indices

$$k, l \in \{1, 2, \cdots, d\} \quad \text{such that} \quad \phi_k = \frac{1}{\overline{\phi_l}}. \tag{22}$$

Proof: The multidimensional TLS problem $\boldsymbol{C}_1\boldsymbol{\Psi} \approx \boldsymbol{C}_2$ can be solved through an SVD of

$$[\boldsymbol{C}_1 \quad \boldsymbol{C}_2] = [\boldsymbol{U}_1 \quad \boldsymbol{U}_2]\begin{bmatrix} \boldsymbol{\Sigma}_1 & \\ & \boldsymbol{\Sigma}_2 \end{bmatrix}\begin{bmatrix} \boldsymbol{V}_{11}^H & \boldsymbol{V}_{21}^H \\ \boldsymbol{V}_{12}^H & \boldsymbol{V}_{22}^H \end{bmatrix}.$$

Then, the TLS solution is obtained from the d right singular vectors corresponding to the d smallest singular values according to

$$\Psi_{\mathrm{TLS}} = -\boldsymbol{V}_{12}\boldsymbol{V}_{22}^{-1} \tag{23}$$

where we have assumed that $\boldsymbol{V}_{22} \in \mathrm{GL}(d)$, i.e., the TLS solution is unique. For the singular case, the reader is referred to [21].

Thus, the TLS problem associated with Unitary ESPRIT can be solved through an SVD of

$$[\boldsymbol{C}_1 \quad \boldsymbol{C}_2] \overset{(19)}{=} [\boldsymbol{C}_1 \quad \boldsymbol{\Pi}_m \overline{\boldsymbol{C}}_1].$$

Notice that this matrix has the same structure as

$$\tilde{\boldsymbol{Z}} = [\tilde{\boldsymbol{X}} \quad \boldsymbol{\Pi}_M \overline{\tilde{\boldsymbol{X}}}].$$

Using, therefore, the same reasoning as in (20) and (21), the TLS problem is solved by computing an SVD of the real matrix

$$\mathcal{T}(\boldsymbol{C}_1) = \boldsymbol{Q}_m^H [\boldsymbol{C}_1 \quad \boldsymbol{\Pi}_m \overline{\boldsymbol{C}}_1]\begin{bmatrix} \boldsymbol{I}_d & \\ & \boldsymbol{\Pi}_d \end{bmatrix} \boldsymbol{Q}_{2d}. \tag{24}$$

Its right singular vectors will be denoted by

$$\boldsymbol{W} = \begin{bmatrix} \boldsymbol{W}_{11} & \boldsymbol{W}_{12} \\ \boldsymbol{W}_{21} & \boldsymbol{W}_{22} \end{bmatrix} \in \mathbb{R}^{2d\times 2d}.$$

Then, the right singular vectors of $[\boldsymbol{C}_1 \quad \boldsymbol{C}_2]$ are determined from

$$\boldsymbol{V}^H = \begin{bmatrix} \boldsymbol{V}_{11}^H & \boldsymbol{V}_{21}^H \\ \boldsymbol{V}_{12}^H & \boldsymbol{V}_{22}^H \end{bmatrix} = \boldsymbol{W}^H \boldsymbol{Q}_{2d}^H \begin{bmatrix} \boldsymbol{I}_d & \\ & \boldsymbol{\Pi}_d \end{bmatrix} \tag{25}$$

and Ψ_{TLS} is obtained from (23). Since the matrix $\boldsymbol{Q}_{2d}\boldsymbol{W}$ is left $\boldsymbol{\Pi}$-real, it can be written as

$$\boldsymbol{Q}_{2d}\boldsymbol{W} = \begin{bmatrix} \boldsymbol{V}_1 \\ \boldsymbol{\Pi}_d \overline{\boldsymbol{V}}_1 \end{bmatrix}$$

for some matrix $\boldsymbol{V}_1 \in \mathbb{C}^{d\times 2d}$, cf. (2). With (25) we, therefore, conclude $\boldsymbol{V}_{22} = \overline{\boldsymbol{V}}_{12}$. Thus, if ϕ_l is an eigenvalue of the TLS solution $\Psi_{\mathrm{TLS}} \in \mathrm{GL}(d)$, $1/\overline{\phi_l}$ is an eigenvalue of

$$\overline{\Psi}_{\mathrm{TLS}}^{-1} = -\boldsymbol{V}_{12}\overline{\boldsymbol{V}}_{12}^{-1} = \Psi_{\mathrm{TLS}}$$

which proves (22). ■

Proposition 3—Eigenvalue Decomposition: The eigenvalues of the complex matrix Ψ_{TLS} can be determined from the eigenvalues of a real matrix of size $d \times d$ via the linear fractional transformation

$$f(x) = -\frac{x - j}{x + j}. \tag{26}$$

Moreover, the eigenvectors of both matrices are identical.

Proof: a) Assume, for the moment, that the left $\boldsymbol{\Pi}$-real matrix $\boldsymbol{Q}_{2d}$ is the one we have defined in (3). Then, (25) yields

$$\begin{aligned}\boldsymbol{V} &= \begin{bmatrix} \boldsymbol{I}_d & \\ & \boldsymbol{\Pi}_d \end{bmatrix} \boldsymbol{Q}_{2d} \boldsymbol{W} \\ &= \frac{1}{\sqrt{2}} \begin{bmatrix} \boldsymbol{I}_n & j\boldsymbol{I}_n \\ \boldsymbol{I}_n & -j\boldsymbol{I}_n \end{bmatrix} \boldsymbol{W}.\end{aligned}$$

After partitioning $\boldsymbol{V}$ and $\boldsymbol{W}$ as before, we therefore conclude from (23)

$$\begin{aligned}\Psi_{\mathrm{TLS}} &= -(\boldsymbol{W}_{12} + j\boldsymbol{W}_{22})(\boldsymbol{W}_{12} - j\boldsymbol{W}_{22})^{-1} \\ &= -((-\boldsymbol{W}_{12}\boldsymbol{W}_{22}^{-1}) - j\boldsymbol{I}_d)((-\boldsymbol{W}_{12}\boldsymbol{W}_{22}^{-1}) + j\boldsymbol{I}_d)^{-1} \\ &= f(\boldsymbol{\Upsilon}_{\mathrm{TLS}}) \qquad \text{with} \quad \boldsymbol{\Upsilon}_{\mathrm{TLS}} = -\boldsymbol{W}_{12}\boldsymbol{W}_{22}^{-1}. \end{aligned} \tag{27}$$

Here, $f(x)$ denotes the linear fractional transformation (26), which is analytic for $x \neq -j$. Let

$$\boldsymbol{\Upsilon}_{\mathrm{TLS}} = -\boldsymbol{W}_{12}\boldsymbol{W}_{22}^{-1} = \boldsymbol{T}\boldsymbol{\Omega}\boldsymbol{T}^{-1} \tag{28}$$

be the eigenvalue decomposition (EVD) of the real matrix $\boldsymbol{\Upsilon}_{\mathrm{TLS}}$. It is a well-known result from function theory that the eigenvalues of Ψ_{TLS} can be obtained through the same linear fractional transformation, i.e.

$$\hat{\boldsymbol{\Phi}} = f(\boldsymbol{\Omega}) \quad \text{with} \quad \boldsymbol{\Omega} = \mathrm{diag}\{\omega_k\}_{k=1}^{d} \quad \text{and} \quad \omega_k \neq -j$$

and the corresponding eigenvectors of $\boldsymbol{\Upsilon}_{\mathrm{TLS}}$ and Ψ_{TLS} are identical.

b) An arbitrary left $\boldsymbol{\Pi}$-real matrix of dimension $2d \times 2d$ can, obviously, be written as

$$\tilde{\boldsymbol{Q}}_{2d} = \boldsymbol{Q}_{2d}\boldsymbol{R}_{2d} \quad \text{where} \quad \boldsymbol{R}_{2d} \in \mathbb{R}^{2d \times 2d}.$$

After replacing the real matrix $\boldsymbol{W}$ by $\tilde{\boldsymbol{W}} = \boldsymbol{R}_{2d}\boldsymbol{W}$, we invoke the same reasoning as above to prove this proposition for an arbitrary left $\boldsymbol{\Pi}$-real transformation $\tilde{\boldsymbol{Q}}_{2d}$. ■

Remark 1—Covariance Approach: Instead of the described square root (or direct data) approach based on a real-valued SVD, cf. Proposition 1, we can use a covariance approach based on a real-valued EVD to determine the signal subspace estimate. Then, $\boldsymbol{E}_s \in \mathbb{R}^{M \times d}$ denotes the d principal eigenvectors of

$$\mathcal{T}(\tilde{\boldsymbol{X}})\mathcal{T}(\tilde{\boldsymbol{X}})^H \in \mathbb{R}^{M \times M}. \tag{29}$$

First, forming $\mathcal{T}(\tilde{\boldsymbol{X}})$ according to (7), followed by the computation of (29), is more efficient than the approach alternative suggested in [8] and [24]. There, it is proposed to compute the complex-valued sample covariance matrix $\boldsymbol{R}_{XX} = \tilde{\boldsymbol{X}}\tilde{\boldsymbol{X}}^H \in \mathbb{C}^{M \times M}$ first. Then, $\boldsymbol{E}_s$ is determined from the EVD of $\mathrm{Re}\{\boldsymbol{Q}_M^H \boldsymbol{R}_{XX} \boldsymbol{Q}_M\}$, which is computationally more expensive than using (29).

C. Reliability Test

Proposition 2 states that the eigenvalues of Ψ_{TLS}, i.e., the phase factors estimated via Unitary ESPRIT, are symmetric with respect to the unit circle, since they satisfy (22). This observation gives rise to a *new reliability test* provided by Unitary ESPRIT without demanding additional computations. This reliability test is a substantial improvement of current high-resolution array signal processing and spectral estimation techniques since usually there is no easy way to determine how reliable the resulting estimates are. Unreliable estimation results might have been caused by a false estimate of the number of sources d or by the fact that there is no source signal at all (only noise).

Remark 2—Eigenvalues with Unit Modulus: Notice first that the eigenvalues ϕ_k that lie on the unit circle form a subset with nonzero measure in the class of all eigenvalues fulfilling (22), i.e., being symmetric with respect to the unit circle. Owing to this and the fact that Unitary ESPRIT produces consistent DOA estimates, asymptotically all the estimated phase factors ϕ_k will be on the unit circle.

If, however, the number of snapshots N is too small or if there is only noise present, the eigenvalues of Ψ_{TLS} might fail to satisfy

$$|\phi_k| = 1 \quad \forall k \tag{30}$$

which indicates that the subsequent estimates will be unreliable. Hence, no further computations should be carried out. Condition (30) implies that all eigenvalues ω_k of $\boldsymbol{\Upsilon}_{\mathrm{TLS}}$ are real, cf. (26).[4] Thus, if some of the ω_k occur in complex conjugate pairs, the Unitary ESPRIT reliability test has failed, and the algorithm has to be restarted with an increased window length N or more reliable measurements. If, conversely, all eigenvalues ω_k are real, i.e., the reliability test has been "passed," all estimated phase factors ϕ_k are precisely on the unit circle.

D. Real-Valued Least Squares

Notice that the derivation of the Unitary ESPRIT reliability test is based on a *total least squares* solution of (16). Thus, the computation of $\boldsymbol{\Upsilon}_{\mathrm{TLS}}$ requires an SVD (or another rank revealing factorization) of $\mathcal{T}(\boldsymbol{C}_1) \in \mathbb{R}^{m \times 2d}$. By computing the less expensive *least squares* instead of the *total least squares* solution of (16), we would, however, lose the benefits of the reliability test, since (22) would no longer be satisfied. Moreover, the complex-valued *least squares* problem (16) cannot be transformed into a real-valued problem of the *same* size. The following remark, however, sets up a different, real-valued *least squares* problem, which can be solved instead.

Remark 3—Least Squares Estimate: After partitioning the real matrix of (24) according to

$$\mathcal{T}(\boldsymbol{C}_1) \stackrel{\mathrm{def}}{=} [\boldsymbol{T}_1\ \boldsymbol{T}_2] \quad \text{with} \quad \boldsymbol{T}_1, \boldsymbol{T}_2 \in \mathbb{R}^{m \times d}$$

[4] Recall that the eigenvalues of a real matrix can either be real or they occur in complex conjugate pairs.

it is easy to see that $\boldsymbol{\Upsilon}_{\mathrm{TLS}}$ is a TLS solution of the real-valued system of equations

$$\boldsymbol{T}_1\boldsymbol{\Upsilon} \approx \boldsymbol{T}_2. \tag{31}$$

To save computations, we can, therefore, solve (31) by computing its *least squares* solution $\boldsymbol{\Upsilon}_{\mathrm{LS}}$. Here, the Unitary ESPRIT reliability test is still applicable, since the resulting matrix $\boldsymbol{\Upsilon}_{\mathrm{LS}}$ is always real. If the reliability test has been "passed", the estimated phase factors are on the unit circle.

The real-valued LS or TLS problem (31) can directly be obtained from $\boldsymbol{E}_s$ by observing

$$\begin{aligned}\mathcal{T}(\boldsymbol{C}_1) &= \boldsymbol{Q}_m^H[\boldsymbol{C}_1 \quad \boldsymbol{C}_2]\begin{bmatrix}\boldsymbol{I}_d & \\ & \boldsymbol{\Pi}_d\end{bmatrix}\boldsymbol{Q}_{2d} \\ &= \boldsymbol{Q}_m^H[\boldsymbol{J}_1\boldsymbol{Q}_M\boldsymbol{E}_s \quad \boldsymbol{J}_2\boldsymbol{Q}_M\boldsymbol{E}_s]\frac{1}{\sqrt{2}}\begin{bmatrix}\boldsymbol{I}_n & j\boldsymbol{I}_n \\ \boldsymbol{I}_n & -j\boldsymbol{I}_n\end{bmatrix} \\ &= \frac{1}{\sqrt{2}}[\boldsymbol{K}_1\boldsymbol{E}_s \quad \boldsymbol{K}_2\boldsymbol{E}_s]\end{aligned}$$

where the selection matrices $\boldsymbol{K}_1$ and $\boldsymbol{K}_2$ are defined as follows:

$$\begin{aligned}\boldsymbol{K}_1 &= \boldsymbol{Q}_m^H\underbrace{(\boldsymbol{J}_1 + \boldsymbol{\Pi}_m\boldsymbol{J}_1\boldsymbol{\Pi}_M)}\boldsymbol{Q}_M \\ \boldsymbol{K}_2 &= \boldsymbol{Q}_m^H\underbrace{j(\boldsymbol{J}_1 - \boldsymbol{\Pi}_m\boldsymbol{J}_1\boldsymbol{\Pi}_M)}\boldsymbol{Q}_M.\end{aligned} \tag{32}$$

Since the matrices in braces are centro-Hermitian, $\boldsymbol{K}_1$ and $\boldsymbol{K}_2$ are always real, cf. Theorem 1. They are even sparse if the selection matrix $\boldsymbol{J}_1$ is sparse and the matrices $\boldsymbol{Q}_m$ and $\boldsymbol{Q}_M$ are chosen according to (3) or (4). This is illustrated by the following example. For the ULA with maximum overlap sketched in Fig. 2(a), $\boldsymbol{J}_1$ is given by

$$\boldsymbol{J}_1 = \begin{bmatrix}1 & 0 & 0 & 0 & 0 & 0 \\ 0 & 1 & 0 & 0 & 0 & 0 \\ 0 & 0 & 1 & 0 & 0 & 0 \\ 0 & 0 & 0 & 1 & 0 & 0 \\ 0 & 0 & 0 & 0 & 1 & 0\end{bmatrix}.$$

Thus, straightforward calculations yield

$$\boldsymbol{K}_1 = \begin{bmatrix}1 & 1 & 0 & 0 & 0 & 0 \\ 0 & 1 & 1 & 0 & 0 & 0 \\ 0 & 0 & \sqrt{2} & 0 & 0 & 0 \\ 0 & 0 & 0 & 1 & 1 & 0 \\ 0 & 0 & 0 & 0 & 1 & 1\end{bmatrix}$$

$$\boldsymbol{K}_2 = \begin{bmatrix}0 & 0 & 0 & -1 & 1 & 0 \\ 0 & 0 & 0 & 0 & -1 & 1 \\ 0 & 0 & 0 & 0 & 0 & -\sqrt{2} \\ 1 & -1 & 0 & 0 & 0 & 0 \\ 0 & 1 & -1 & 0 & 0 & 0\end{bmatrix}.$$

E. Summary of the Algorithm

Before presenting a summary of Unitary ESPRIT, we note an interesting relationship between the eigenvalues of the real matrix $\boldsymbol{\Upsilon}$ denoted by ω_k, and the estimated phase factors $\phi_k = e^{j\mu_k}$, cf. (9). Solving $e^{j\mu_k} = f(\omega_k)$ for the spatial frequencies μ_k yields the simple expression

$$\mu_k = \frac{1}{j}\ln\left(\frac{1+j\omega_k}{1-j\omega_k}\right) = 2\arctan\,\omega_k, \qquad k = 1, 2, \cdots, d. \tag{33}$$

Now, we are in the position to summarize the described real implementation of Unitary ESPRIT, which is given in Table I. Here, the left $\boldsymbol{\Pi}$-real matrices $\boldsymbol{Q}_m$ and $\boldsymbol{Q}_M$ are chosen according to (3) or (4).

Notice that a linear estimate of the source signal matrix $\boldsymbol{S}$ (Step 7) can easily be obtained by applying the results of this section to the source signal matrix estimate derived in [4], where (without loss of generality) the additive noise is assumed to be spatially uncorrelated.

V. Computer Simulations

In this section, we present some simulation results that compare Unitary ESPRIT with the standard ESPRIT algorithm, using the SVD implementation in all cases. Among others, we examine scenarios where the standard ESPRIT algorithm faces some problems, like low signal-to-noise ratios, short window lengths, and correlated source signals.

A. Signal Reconstruction

First, we examine the effect of Unitary ESPRIT on the resulting signal estimates. To this end, three impinging wavefronts are reconstructed using a single ULA of $M = 9$ sensors with maximum overlap, cf. Fig. 2(a). The three uncorrelated equi-powered QPSK signals arrive from $\theta_1 = 10°, \theta_2 = 20°$, and $\theta_3 = 30°$, respectively. Fig. 3 depicts the resulting output signal-to-noise-and-interference ratio (SNIR) as a function of the SNR and the number of snapshots N using standard ESPRIT (dashed lines) and Unitary ESPRIT (solid lines). The values of N marked on the right side of the figure correspond to the solid lines, i.e., Unitary ESPRIT. The output SNIR achieved by the standard ESPRIT algorithm for a given value of N (dashed lines) can be found below the corresponding solid lines. For small values of N, e.g., $N = 5$ snapshots, Unitary ESPRIT achieves a significantly better performance than the standard ESPRIT algorithm. Notice that standard ESPRIT with $N = 10$ snapshots attains the same performance as Unitary ESPRIT with $N = 5$ snapshots for SNR's that are greater than 15 dB, while the performance of standard ESPRIT with $N = 20$ is comparable to the performance of Unitary ESPRIT with $N = 10$ for SNR's that are greater than 5 dB. Thus, Unitary ESPRIT essentially doubles the number of available snapshots N compared to the standard ESPRIT algorithm.

B. DOA Estimation

Next, we investigate the effect of Unitary ESPRIT on the estimated phase factors $\phi_k, 1 \le k \le d$. Consider a ULA with $M = 6$ sensors and three correlated signals impinging from $\theta_1 = -20°, \theta_2 = 0°$, and $\theta_3 = 20°$. Their correlation matrix is given by

$$\boldsymbol{R}_{xx} = \begin{bmatrix}1 & \rho & \rho \\ \rho & 1 & \rho^2 \\ \rho & \rho^2 & 1\end{bmatrix}. \tag{34}$$

The phase factors ϕ_1, ϕ_2, and ϕ_3, estimated with the standard ESPRIT algorithm and Unitary ESPRIT, are marked by crosses (+) in the complex plane as depicted in Figs. 4 and 5 for

TABLE I
SUMMARY OF UNITARY ESPRIT

1. *Initialization:* Form the matrix $\widetilde{\boldsymbol{X}} \in \mathbf{C}^{M \times N}$ from the available measurements.
2. *Signal Subspace Estimation:* Determine the real matrix $\mathcal{T}(\widetilde{\boldsymbol{X}}) \in \mathbf{R}^{M \times 2N}$ from (7), and compute the SVD of $\mathcal{T}(\widetilde{\boldsymbol{X}})$ (square root approach) or the eigendecomposition of $\mathcal{T}(\widetilde{\boldsymbol{X}})\mathcal{T}(\widetilde{\boldsymbol{X}})^H$ (covariance approach). The d dominant left singular vectors or eigenvectors will be called $\boldsymbol{E}_s \in \mathbf{R}^{M \times d}$. Estimate the number of sources d, if d is not known a priori [22].
3. *(Total) Least Squares:* Solve the overdetermined system of equations
$$\boldsymbol{K}_1 \boldsymbol{E}_s \boldsymbol{\Upsilon} \approx \boldsymbol{K}_2 \boldsymbol{E}_s$$
by means of *least squares* (or *total least squares*) techniques. The selection matrices $\boldsymbol{K}_1$ and $\boldsymbol{K}_2$ are defined in (32).
4. *Eigenvalue Decomposition:* Compute the eigendecomposition of the resulting solution
$$\boldsymbol{\Upsilon} = \boldsymbol{T}\boldsymbol{\Omega}\boldsymbol{T}^{-1} \in \mathbf{R}^{d \times d}, \quad \text{where} \quad \boldsymbol{\Omega} = \operatorname{diag}\{\omega_k\}_{k=1}^{d}.$$
5. *Reliability Test:* If all eigenvalues ω_k are real, the estimates will be reliable. Otherwise, start again with more measurements.
6. *DOA Estimation:* Estimate the directions of arrival (DOA's) from
$$\mu_k = 2 \arctan \omega_k, \quad k = 1, 2, \ldots, d,$$
according to (9).
7. *Signal Reconstruction:* A linear estimate of the source signal matrix $\boldsymbol{S} \in \mathbf{C}^{d \times N}$ is given by
$$\widehat{\boldsymbol{S}} = \left(\boldsymbol{D}\boldsymbol{T}^{-1}\boldsymbol{E}_s^H \boldsymbol{Q}_M^H\right)\widetilde{\boldsymbol{X}},$$
where $\boldsymbol{D} \in \mathbf{C}^{d \times d}$ denotes an arbitrary diagonal (row) scaling matrix [4].

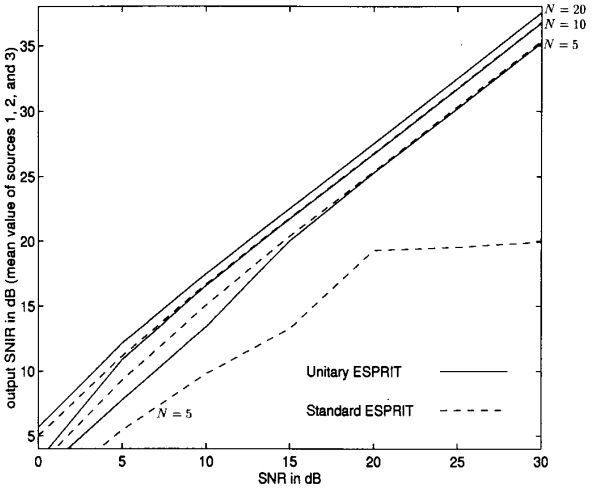

Fig. 3. Output SNIR as a function of the SNR and the number of snapshots N using standard ESPRIT (dashed lines) and Unitary ESPRIT (solid lines) for $\theta_1 = 10°, \theta_2 = 20°$, and $\theta_3 = 30°$ ($M = 9$ sensors, 1000 trial runs). The values of N marked on the right side of the figure correspond to the solid lines, i.e., Unitary ESPRIT. The output SNIR achieved by the standard ESPRIT algorithm for a given value of N (dashed lines) can be found below the corresponding solid lines.

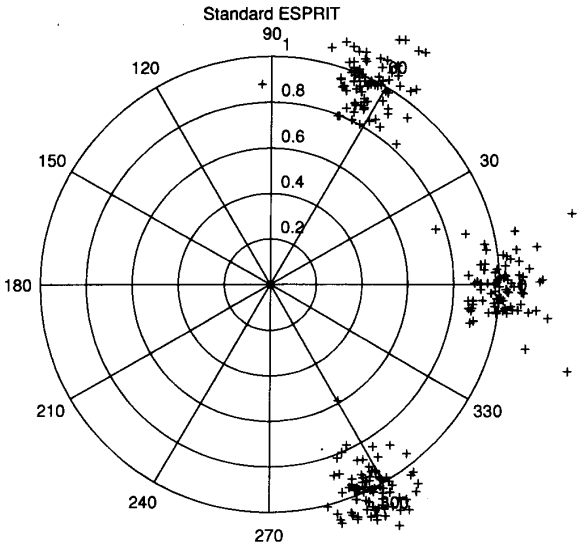

Fig. 4. Phase factors ϕ_1, ϕ_2, and ϕ_3, estimated with the standard ESPRIT algorithm for $\theta_1 = -20°, \theta_2 = 0°, \theta_3 = 20°$, and correlation coefficients $\rho_{12} = 0.5, \rho_{13} = 0.5$, and $\rho_{23} = 0.25$ ($M = 6$ sensors, SNR = 0 dB, $N = 20$, 80 trial runs).

a correlation coefficient of $\rho = 0.5$. The results of 80 trial runs with $N = 20$ snapshots and an SNR of 0 dB are shown. Notice that all phase factors estimated with Unitary ESPRIT are precisely on the unit circle (Fig. 5). Figs. 6 and 7 depict the estimated phase factors for a correlation coefficient of $\rho = 0.8$. In this example, the Unitary ESPRIT reliability test has failed three times. To picture these failures, the corresponding phase factor estimates are surrounded by circles (○), cf. Fig. 7. Notice that the variance of the DOA estimates that pass the Unitary ESPRIT reliability test is much

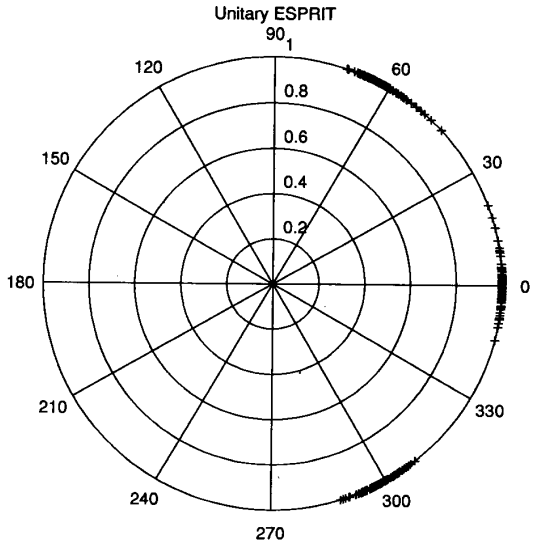

Fig. 5. Phase factors ϕ_1, ϕ_2, and ϕ_3, estimated with Unitary ESPRIT for $\theta_1 = -20°, \theta_2 = 0°, \theta_3 = 20°$, and correlation coefficients $\rho_{12} = 0.5, \rho_{13} = 0.5$, and $\rho_{23} = 0.25$ ($M = 6$ sensors, SNR = 0 dB, $N = 20$, 80 trial runs).

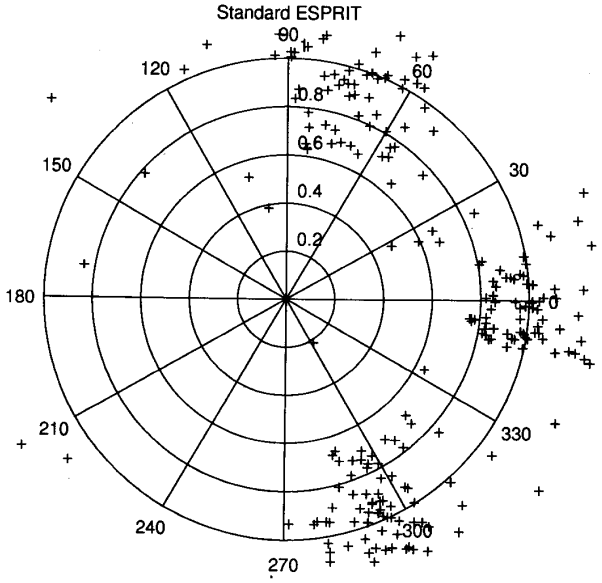

Fig. 6. Phase factors ϕ_1, ϕ_2, and ϕ_3, estimated with the standard ESPRIT algorithm for $\theta_1 = -20°, \theta_2 = 0°, \theta_3 = 20°$, and correlation coefficients $\rho_{12} = 0.8, \rho_{13} = 0.8$, and $\rho_{23} = 0.64$ ($M = 6$ sensors, SNR = 0 dB, $N = 20$, 80 trial runs).

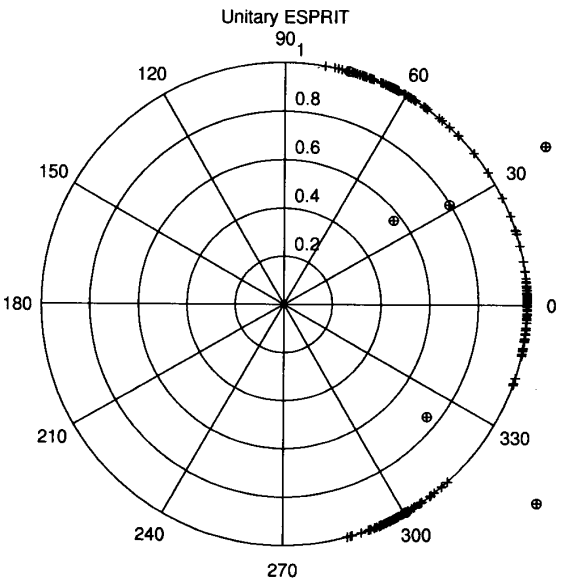

Fig. 7. Phase factors ϕ_1, ϕ_2, and ϕ_3, estimated with Unitary ESPRIT for $\theta_1 = -20°, \theta_2 = 0°, \theta_3 = 20°$, and correlation coefficients $\rho_{12} = 0.8, \rho_{13} = 0.8$, and $\rho_{23} = 0.64$ ($M = 6$ sensors, SNR = 0 dB, $N = 20$, 80 trial runs). Estimates that produced a failure of the reliability test are surrounded by a circle (o).

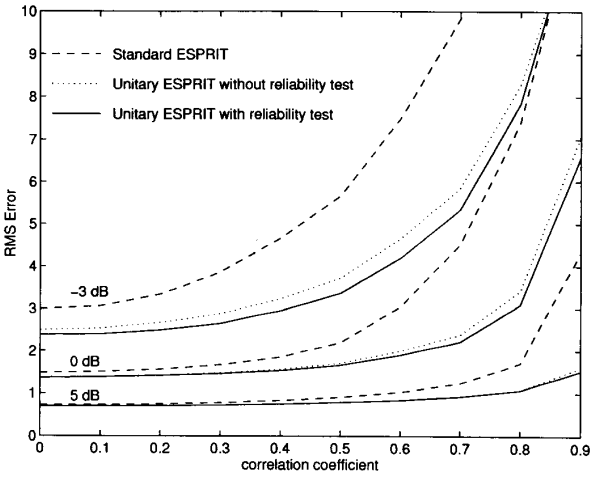

Fig. 8. Root mean squared error (RMSE) in degrees of the estimated directions of arrival as a function of the correlation coefficient ρ and the SNR for $\theta_1 = -20°, \theta_2 = 0°$, and $\theta_3 = 20°$($M = 6$ sensors, $N = 20$, 3000 trial runs). The signal correlation matrix is given by (34).

lower than the variance of the DOA estimates obtained by the standard ESPRIT approach. The advantages of Unitary ESPRIT become even more evident if the root mean squared error (RMSE) of the estimated directions of arrival is plotted as a function of the correlation coefficient ρ. Fig. 8 show these curves for SNR's of -3, 0, and 5 dB using 3000 trial runs. The standard ESPRIT algorithm (dashed line - - -) is compared with Unitary ESPRIT without reliability test (dotted line $\cdots$), and Unitary ESPRIT with the new reliability test (solid line —). It can be seen that Unitary ESPRIT improves the estimation accuracy considerably. In the case of low SNR's, the estimation accuracy is improved even further, by exploiting the information provided by the new reliability test. The corresponding failure rates of the Unitary ESPRIT reliability test are plotted in Fig. 9.

Due to the forward-backward averaging effect, Unitary ESPRIT can separate two completely coherent wavefronts, which is demonstrated in the next example. Two correlated

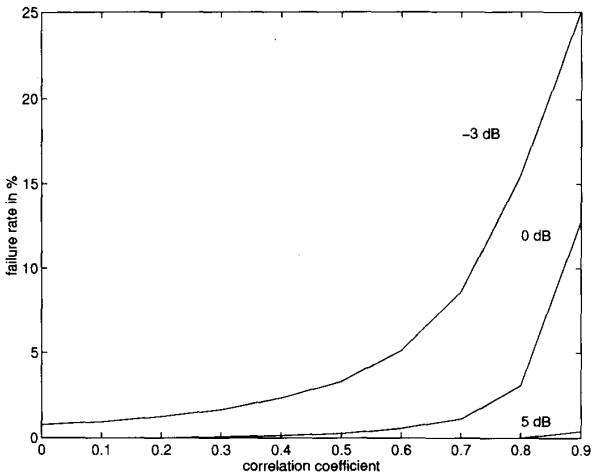

Fig. 9. Failures of the Unitary ESPRIT reliability test as a function of the correlation coefficients ρ for $\theta_1 = -20°, \theta_2 = 0°$, and $\theta_3 = 20°$ ($M = 6$ sensors, $N = 20$, 3000 trial runs). Once again, the signal correlation matrix is given by (34). These curves correspond to the solid lines in Fig. 8.

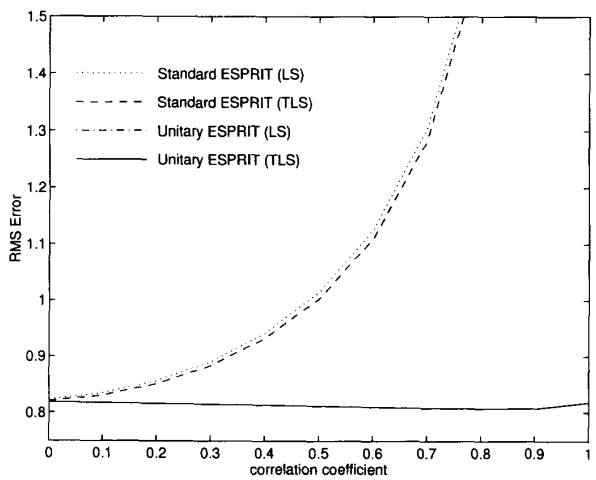

Fig. 10. RMSE (in degrees) of the estimated directions of arrival as a function of the correlation coefficient ρ for $\theta_1 = 0°$ and $\theta_2 = 20°$($M = 4$ sensors, $N = 20$, 100 trial runs). Notice that the curves for the LS and the TLS version of Unitary ESPRIT fall on top of one another.

signals with correlation coefficient ρ are impinging an a ULA of $M = 4$ sensors from $\theta_1 = 0°$and $\theta_2 = 20°$. Fig. 10 shows the resulting RMS error of the estimated DOA's as a function of ρ. The performance of Unitary ESPRIT is not effected by the correlation, while the performance of standard ESPRIT deteriorates dramatically as ρ increases. Notice also that the difference between TLS and LS version of standard ESPRIT is negligible, while the LS and the TLS version of Unitary ESPRIT fall on top of one another. Thus, it is advisable to use the LS version of Unitary ESPRIT instead of the computationally more expensive TLS version. Finally, Figs. 11 and 12 show the RMS error of the estimated DOA's as a function of the magnitude and phase of a complex-valued correlation coefficient ρ, confirming the conclusions drawn from Fig. 10.

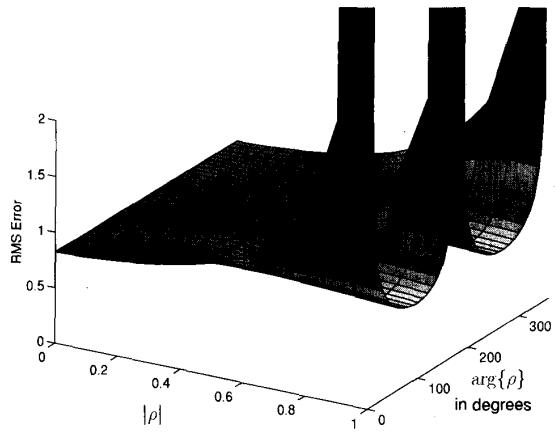

Fig. 11. RMSE (in degrees) of the estimated directions of arrival as a function of the magnitude and phase of the complex correlation coefficient ρ for $\theta_1 = 0°$ and $\theta_2 = 20°$ using standard ESPRIT ($M = 4$ sensors, $N = 20$, 100 trial runs).

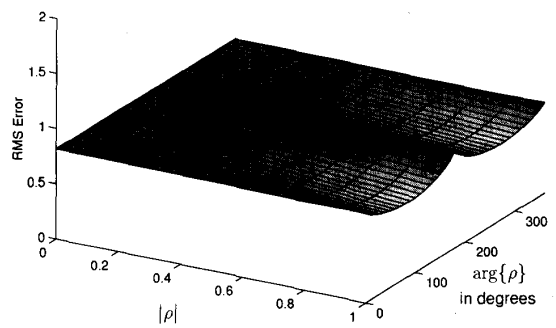

Fig. 12. RMSE (in degrees) of the estimated directions of arrival as a function of the magnitude and phase of the complex correlation coefficient ρ for $\theta_1 = 0°$ and $\theta_2 = 20°$ using Unitary ESPRIT ($M = 4$ sensors, $N = 20$, 100 trial runs).

VI. Concluding Remarks

An improved version of the ESPRIT algorithm, called Unitary ESPRIT, has been presented in this paper. Unitary ESPRIT represents a simple method to constrain the estimated phase factors to the unit circle, yielding more accurate signal subspace estimates. The computational complexity is reduced significantly by exploiting the one-to-one correspondence between centro-Hermitian and real matrices, allowing a transformation to real matrices, which can be maintained for all steps of the algorithm. Unitary ESPRIT also provides a new reliability test, which is particularly useful in extremely low SNR's. Due to the inherent forward-backward averaging effect, Unitary ESPRIT can separate two completely coherent sources and provides improved estimates for correlated signals. Moreover, Unitary ESPRIT offers a great potential to improve the performance of approximate signal subspace estimation techniques, which are well suited for an adaptive implementation, since inexpensive updating strategies are known [5].

The fact that Unitary ESPRIT is efficiently formulated in terms of real-valued computations from start to finish, is

critically important for the extension to 2-D centro-symmetric arrays with a dual invariance structure. 2-D Unitary ESPRIT [23] provides automatically paired source azimuth and elevation angle estimates along with an efficient way to reconstruct the impinging wavefronts. Furthermore, an efficient DFT beamspace implementation of Unitary ESPRIT has also been derived in [23], enabling reduced dimension processing in beamspace, if there is *a priori* information on the general angular location of the DOA's.

ACKNOWLEDGMENT

The authors would like to thank Prof. M. Viberg, Gothenburg, Sweden, for his helpful comments regarding the contents of this paper.

REFERENCES

[1] C. H. Bischof and G. M. Shroff, "On updating signal subspaces," *IEEE Trans. Signal Processing*, vol. 40, pp. 96–105, Jan. 1992.
[2] T. F. Chan, "Rank revealing QR factorization," *Linear Algebra and its Applications*, vol. 88, 89, pp. 67–82, 1987.
[3] J. Götze and A. J. van der Veen, "On-line subspace estimation using a Schur-type method," *IEEE Trans. Signal Processing*, Nov. 1993, submitted for publication.
[4] M. Haardt and M. E. Ali-Hackl, "Unitary ESPRIT: How to exploit additional information inherent in the rotational invariance structure," in *Proc. IEEE Int. Conf. Acoust., Speech, Signal Processing*, Adelaide, Australia, Apr. 1994, pp. 229–232, vol. IV.
[5] M. Haardt and J. Götze, "Unitary Schur–type subspace estimation," Technical University of Munich, Inst. of Network Theory Circuit Design, Munich, Germany, Tech. Rep. TUM-LNS-TR-94-6, July 1994.
[6] M. Haardt, P. Weismüller, and R. Killmann, "The identification of late fields: A multichannel high-resolution state space approach," in *Proc. 14th GRETSI Symp. Signal Image Processing*, Juan-les-Pins, France, Sept. 1993, pp. 1251–1254.
[7] Y. Hua and T. K. Sarkar, "On SVD for estimating generalized eigenvalues of singular matrix pencil in noise," *IEEE Trans. Signal Processing*, vol. 39, pp. 892–900, Apr. 1991.
[8] K. C. Huarng and C. C. Yeh, "A unitary transformation method for angle-of-arrival estimation," *IEEE Trans. Signal Processing*, vol. 39, pp. 975–977, Apr. 1991.
[9] ——, "Adaptive beamforming with conjugate symmetric weights," *IEEE Trans. Antenna. Propagat.*, vol. 39, pp. 926–932, July 1991.
[10] A. Lee, "Centrohermitian and skew-centrohermitian matrices," *Linear Algebra and its Applications*, vol. 29, pp. 205–210, 1980.
[11] K. J. R. Liu, D. P. O'Leary, G. W. Stewart, and Y. J. J. Wu, "An adaptive ESPRIT based on URV decomposition," in *Proc. IEEE Int. Conf. Acoust., Speech, Signal Processing*, Minneapolis, MN, Apr. 1993, pp. 37–40, vol. IV.
[12] B. Ottersten, M. Viberg, and T. Kailath, "Performance analysis of the total least squares ESPRIT algorithm," *IEEE Trans. Signal Processing*, vol. 39, pp. 1122–1135, May 1991.
[13] S. U. Pillai and B. H. Kwon, "Forward/backward spatial smoothing techniques for coherent signal identification," *IEEE Trans. Acoust., Speech, Signal Processing*, vol. 37, pp. 8–15, Jan. 1989.
[14] B. D. Rao and K. V. S. Hari, "Weighted subspace methods and spatial smoothing: Analysis and comparison," *IEEE Trans. Signal Processing*, vol. 41, pp. 788–803, Feb. 1993.
[15] R. Roy and T. Kailath, "ESPRIT—Estimation of signal parameters via rotational invariance techniques," in *Signal Processing Part II: Control Theory and Applications* (L. Auslander, F. A. Grünbaum, J. W. Helton, T. Kailath, P. Khargonekar, and S. Mitter, Eds.). Berlin, Vienna, New York: Springer-Verlag, 1990, pp. 369–411.
[16] R. Roy, A. Paulraj, and T. Kailath, "ESPRIT—A subspace rotation approach to estimation of parameters of cisoids in noise," *IEEE Trans. Acoust., Speech, Signal Processing*, vol. ASSP-34, pp. 1340–1342, Oct. 1986.
[17] R. H. Roy, "ESPRIT—Estimation of Signal Parameters via Rotational Invariance Techniques," Ph.D. thesis, Stanford Univ., Stanford, CA, Aug. 1987.
[18] G. W. Stewart, "An updating algorithm for subspace tracking," *IEEE Trans. Signal Processing*, vol. 40, pp. 1535–1541, June 1992.
[19] A. J. van der Veen, "A Schur method for low-rank matrix approximation," *SIAM J. Matrix Anal. Appl.*, 1994, accepted for publication.
[20] A. J. van der Veen, E. F. Deprettere, and A. L. Swindlehurst, "Subspace-based signal analysis using singular value decomposition," *Proc. IEEE*, vol. 81, pp. 1277–1308, Sept. 1993.
[21] S. Van Huffel and J. Vandewalle, *The Total Least Squares Problem: Computational Aspects and Analysis Frontiers in Applied Mathematics, Vol. 9.* Philadelphia, PA: Soc. Ind. and Applied Math., 1991.
[22] G. Xu, R. H. Roy, and T. Kailath, "Detection of number of sources via exploitation of centro-symmetry property," *IEEE Trans. Signal Processing*, vol. 42, pp. 102–112, Jan. 1994.
[23] M. D. Zoltowski, M. Haardt, and C. P. Mathews, "Closed-form angle estimation with rectangular arrays in element space or beamspace via Unitary ESPRIT," *IEEE Trans. Signal Processing*, July 1994, submitted for publication.
[24] M. D. Zoltowski, G. M. Kautz, and S. D. Silverstein, "Beamspace Root-MUSIC," *IEEE Trans. Signal Processing*, vol. 41, pp. 344–364, Jan. 1993.

Martin Haardt (S'90) was born in Germany on October 4, 1967 and received the Diplom-Ingenieur degree in electrical engineering from the Ruhr-University Bochum, Germany, in 1991.

From 1989 to 1990, he was a visiting scholar at Purdue University, West Lafayette, IN, USA, sponsored by a fellowship of the German Academic Exchange Service (DAAD). From 1991 to 1993, he worked for Siemens AG, Corporate Research and Development, in Munich, Germany, conducting research in the areas of image processing and biomedical signal processing. Since 1993 he has been a research associate with the Institute of Network Theory and Circuit Design at the Technical University of Munich, Germany, where he is also working toward a Ph.D. degree. His current research interests include array signal processing, spectral estimation, numerical linear algebra, and mobile communications.

Josef A. Nossek (S'72–M'74–SM'81–F'93) was born in Vienna, Austria, on December 17, 1947 and received the Diplom-Ingenieur and the Ph.D. degrees, both in electrical engineering, from the Technical University of Vienna, Austria, in 1974 and 1980, respectively.

In 1974, he joined Siemens AG, Munich, Germany, where he was engaged in the design of passive and active filters for communication systems. In 1978, he became a supervisor, and in 1980 the head of a group of laboratories concerned with the design of monolithic filters (analog and digital) and electromechanical and microwave filters. In 1982, he became head of a group of laboratories designing digital radio systems within the Transmission Systems Department. In 1985, he spent a month as a visiting professor at the University of Cape Town, South Africa. From 1987 to 1989, he was head of the Radio Systems Design Department. Since April 1989, he has been a full professor and head of the Institute of Network Theory and Circuit Design at the Technical University of Munich, Germany. He is teaching undergraduate and graduate courses in the field of circuit and system theory and conducting research in the areas of real-time signal processing, neural networks, and dedicated VLSI-architectures.

Dr. Nossek has published more than 100 papers in scientific and technical journals and conference proceedings. He holds a number of patents. In 1988, he received the ITG best paper award. From 1991 to 1993, he served as an associate editor of the IEEE TRANSACTIONS ON CIRCUITS AND SYSTEMS.